Optimization of the Charge Comparison Method for Multiradiation Field Using Various Measurement Systems

Clément Lynde, Eva Montbarbon, Matthieu Hamel, Amélie Grabowski, Camille Frangville, Guillaume H. V. Bertrand, Giacomo Galli, Frédérick Carrel, Vincent Schoepff, Ziad El Bitar

Optimization of the charge comparison method for multi-radiation field using various measurement systems

C. Lynde, E. Montbarbon, M. Hamel, A. Grabowski, C. Frangville, G. H. V. Bertrand, G. Galli, F. Carrel, V. Schoepff, Z. El Bitar

***Abstract*—This article presents a procedure for optimizing the charge comparison method (CCM) used for pulse shape discrimination (PSD). Without prior knowledge on the signals or the readout system, our procedure automatically optimizes integration periods maximizing the discrimination ability of the radiation detector. This procedure is innovative in its adaptability and automation without being complicated to implement on a standard computer. Another advantage of this approach is the possibility to use it even if the operation of the readout system and the recording process of the signal is not fully known. Therefore, it enables all detection systems generating signals whose temporal evolution depends on the origin to optimize the integration periods of the CCM. Our procedure is based on verifying that two criteria are met in terms of the number of components and the correlation of Gaussian fits made on the distribution of the tail-to-total integral resulting from the CCM. We tested the procedure for different application cases. First, the optimization of the integration periods of the CCM was performed for the discrimination between fast neutrons and gamma rays with a plastic scintillator and a silicon photomultiplier (SiPM) in the energy range [250 keVee; 4.5 MeVee]. The integration periods, from the laboratory's experience with photomultiplier tubes (PMTs) and plastic scintillators, gave a FoM of 0.58 corresponding to a rejection ratio of 8.6%. The procedure improved the FoM up to 0.88 corresponding to a rejection ratio of 1.9%. We also applied the procedure to the discrimination between beta and gamma rays with a PMT and a *phoswich* organic detector and to the discrimination between signals collected from neutrons or partial discharges within a fission chamber.**

***Index Terms*—Particles classification, pulse shape discrimination, charge comparison method, scintillator, fission chamber**

I. Introduction

PULSE-SHAPE discrimination (PSD) is a widely used technique to identify particles by analyzing the electrical signal induced in a detector [1] and in particular with plastic scintillator [2]. Usually, such an electrical signal consists of a succession of pulses, each of them representing the detection of a neutron, X- or γ-rays, β or α particles, or the noise occurrence within the detector. Due to its simplicity and performance, one of the most frequently used PSD method is the charge comparison method (CCM) [3]–[7]. The CCM generally allows the identification of the phenomenon at the origin of each pulse solely based on the value of the tail-to-total integral. This latter involves the integration of each pulse of the detection signal over two different time periods. Since the optimal values are not known in all cases, several solutions have been considered in the literature [8]–[10] to solve this problem. As detailed in Section III.A, these methods were not entirely satisfactory for many applications; therefore, we propose a novel procedure capable of carefully choosing the integration durations.

This paper presents the discrimination principle of the associated measurement system used in it. Then, the pulse shape discrimination processed on signals is detailed. In Section IV, the optimization procedure is explained. Finally, this article presents the improvement due the optimization and focuses on three case studies.

II. Discrimination principle and associated measurement systems

A. Between fast neutrons and gamma rays with organic scintillator

The scintillation mechanism in organic scintillators has been described by Birks [11]. In the case of a charged particle (*e.g.* alpha, beta, proton) or a secondary ionizing particle (mainly proton for neutron and electron for gamma ray), its motion in the material will excite the scintillator whose de-excitation is accompanied by the emission of visible photons. The discrimination between neutrons and gamma rays in scintillators has been theorized by Voltz and Laustriat [12]. The difference between the types of particles, identifiable on the electrical signals, is due to the density of the excited states generated by the ionizing particle. The ionization power of a recoil proton being greater to a recoil electron, the density of

This paragraph of the first footnote will contain the date on which you submitted your paper for review. The Authors are indebted to the French National Agency "ANR" for financial support, within the frame of the Nessyned project (ANR-15-CE39-0006).

C. Lynde, M. Hamel, A. Grabowski, C. Frangville, G. H. V. Bertrand, F. Carrel, and V. Schoepff are with the CEA, LIST, Sensors and Electronic Architectures Laboratory, Gif-sur-Yvette, France (e-mail: clement.lynde@cea.fr).

E. Montbarbon is with the CERN, EN-EA-LE Genève, Switzerland.

G. Galli is with the CentraleSupélec, Group of Electrical Engineering-Paris, Gif-sur-Yvette, France.

Z. El Bitar is with the Institut Pluridisciplinaire Hubert Curien/IN2P3/CNRS, Strasbourg, France.

excitation of the scintillator is therefore more important. The energy deposition of a proton thus generates more delayed de-excitation than that of an electron. As a result, for the same amount of deposited energy, the pulse generated by an interaction with neutrons will be more spread over time than a pulse generated by an interaction with gamma rays (see an example in Fig. 1).

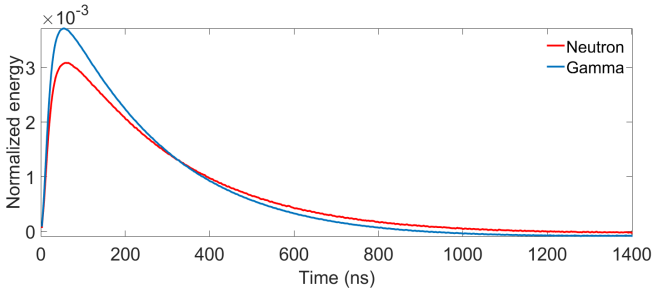

Fig. 1. Baseline-subtracted and energy-normalized average pulses from neutron pulses (red line) and gamma ray pulses (blue line) obtained from a plastic scintillator, a SiPM and a ^{252}Cf source.

In the work presented in this article, two homemade organic scintillators were used:

- A liquid cell (left photograph in Fig. 2), filled with BC-501A liquid scintillator marketed by Saint-Gobain Crystals and Detectors. The surface of the cell was 1.5×1.5 cm^2 and the height 4 cm.
- A plastic scintillator (right photograph in Fig. 2), composed of a high concentration of 2,5-diphenyloxazole and a small quantity of 9,10-diphenylanthracene in polystyrene. This formulation should be closed to that of EJ-276 (formerly EJ-299-33) from Eljen Technology. The diameter of the scintillator was 1.5 cm and the height 1.5 cm.

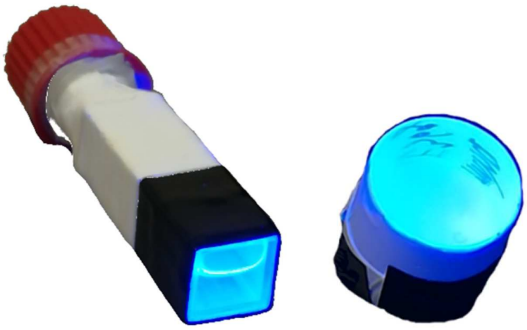

Fig. 2. Overview of the organic scintillators used for these tests and manufactured in the laboratory. Left: BC-501A liquid scintillator. Right: EJ-276 plastic scintillator.

We used two different photosensors to collect the light emitted from those two scintillators:

- A Hamamatsu R7724-100 photomultiplier tube (PMT), left photograph in Fig. 3.
- A SensL ArrayC-30035-16P silicon photomultiplier (SiPM), right photograph in Fig. 3.

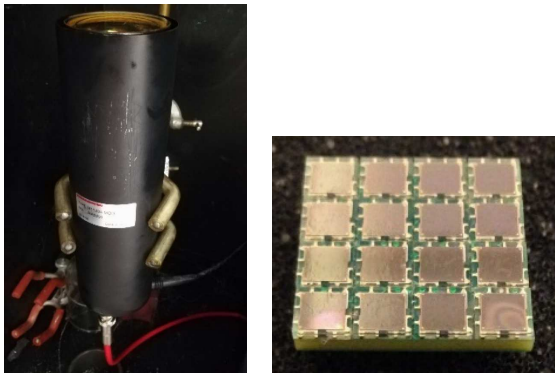

Fig. 3. Overview of the photosensors used. Left: Hamamatsu R7724-100 PMT. Right: SensL ArrayC-30035-16P SiPM.

In this article, the plastic scintillator was tested with both photosensors whereas the liquid scintillator only with the PMT.

B. Between beta and gamma rays with phoswich scintillator

For mixed radiation field, a *phoswich* (phosphor sandwich) detector can also be used [1], [13]–[15]. This kind of detector consists of a combination of two or more layers of dissimilar scintillators optically coupled to only one photodetector. Scintillators must have decay times such that the pulse at the output of the photodetector is dependent on the emitted light. The differences accessible within the pulse will then identify the scintillator(s) in which the interaction occurs. In our case, a two layers *phoswich* plastic scintillator was used (see Fig. 4). The first 0.15 mm layer was composed of the "fast" scintillator EJ-212 (decay time of 2.4 ns) and the second 5 mm layer of the "slow" one EJ-240 (decay time of 285 ns). In order to maximize the light collection and minimize the energy deposition by beta in the reflector material, the surface of the *phoswich* was recovered by polytetrafluoroethylene (PTFE) with an entry window. The *phoswich* detector was optically coupled to the PMT described in the Section A.

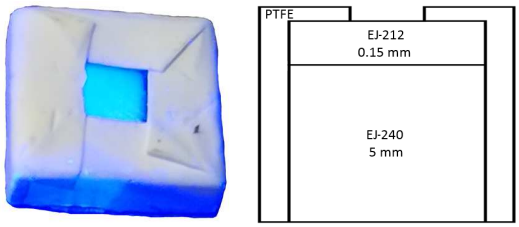

Fig. 4. Overview of the *phoswich* scintillator used. Left: Photograph. Right: Vertical cross-sectional schematic (not to scale).

In this configuration, low-energy betas (< 100 keV) only interact in the first scintillator and induce very short pulses. High-energy betas (> 100 keV) interact in both scintillators and induce pulses with a fast and slow component. Due to the large volume difference (~30×), gamma rays interact mainly and only in the second scintillator and induce long pulses. The representative pulse for each of the three pulse shapes is shown in Fig. 5.

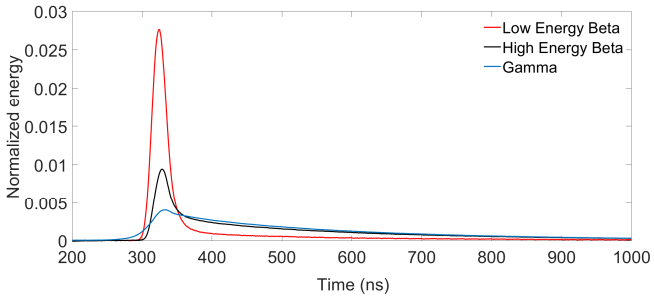

Fig. 5. Baseline-subtracted and energy-normalized average pulses from low-energy beta pulses (red line), high-energy pulses (black line) and gamma ray pulses (blue line) obtained from a *phoswich* plastic scintillator, a PMT, ^{137}Cs and ^{90}Sr/^{90}Y sources.

C. *Between neutrons and partial discharges with fission chamber*

Sodium-cooled fast neutron reactors are among the advanced reactors selected by the Generation IV International Forum. The fission chamber (see Fig. 6) has been identified as the most appropriate neutron detector for use in the vessel of this type of reactor [16]. This detector - namely High Temperature Fission Chamber (HTFC), must be able to operate under high irradiation (up to 10^{10} neutrons.cm^{-2}.s^{-1}) and high temperature (up to 650 °C).

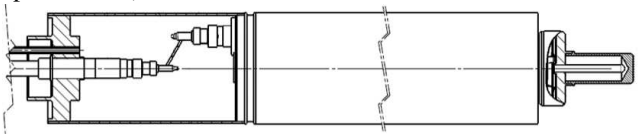

Fig. 6. Simplified schematic of a fission chamber.

One of the effect of this hostile environment is the occurrence of partial discharges (PD). Under given temperature and bias voltage conditions, PD can induce a pulse in fission chambers. The physics underlying creation of PD is still under investigation. Therefore, the rejection of signals induced by this phenomenon has been studied [17]. It has been experimentally proven that the neutron-induced and the partial-discharge-induced signals have temporal differences from which it is possible to discriminate them. The representative pulse for each of the two pulse shapes is shown in Fig. 7.

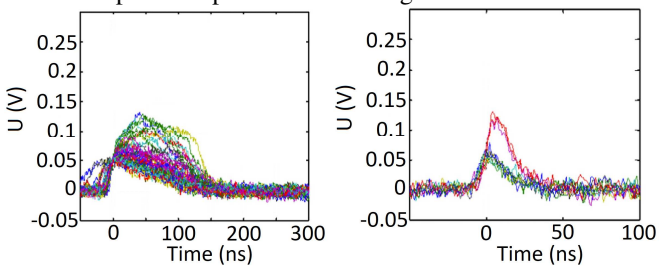

Fig. 7. Representatives pulses obtained with a fission chamber taken from [17]. Left: ^{252}Cf neutron-induced pulses at room temperature. Right: PD-induced pulses at 600 °C.

III. Pulse Shape Discrimination

The required format for input data for the implementation of PSD and our optimization procedure is the temporal evolution of pulse recorded using a digitizer or a digital oscilloscope. Pulse measurements involving scintillators were performed with a CAEN "DT5743" digitizer (500 MHz of bandwidth, 12 bits of resolution) at 800 mega-samples/s with PMT and 400 mega-samples/s with SiPM, and involving fission chambers with a digital LeCroy "wavePro 725Zi" oscilloscope (2.5 GHz of bandwidth, 10 bits of resolution) at 20 giga-samples/s.

A. *Charge comparison method*

The Charge Comparison Method (CCM) is one of the signal processing methods used to perform PSD to discriminate signals according to their origin. The CCM can be applied when observable signals have temporal differences characteristic of their origin. It consists in integrating the pulse, $T(t)$, over two different time periods, a so-called slow period, Q_{slow}, and a so-called total period, Q_{tot} according to (1) and (2). For each pulse, its start, t_{begin}, is evaluated and it is defined as the first time step from which the pulse is greater than 5% of the amplitude. Fig. 8 illustrates the placement of the other two integration gates, t_{fast} and t_{long}.

$$Q_{slow} = \int_{t_{fast}}^{t_{slow}} T(t).dt \quad (1)$$

$$Q_{tot} = \int_{t_{begin}}^{t_{slow}} T(t).dt \quad (2)$$

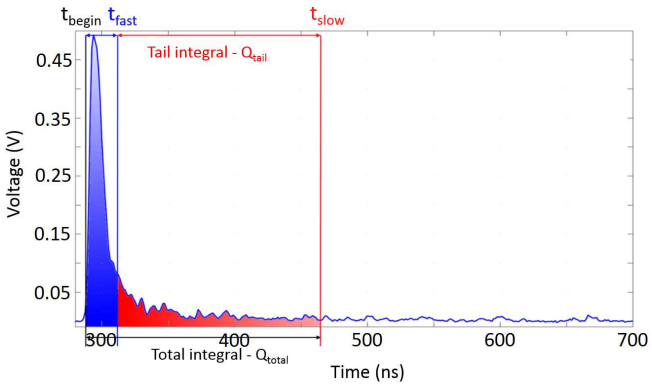

Fig. 8. Example of pulse processing.

The tail-to-total integral used to differentiate the origin of pulses is the ratio, R_{CCM}, of the slow integral to the total integral, defined by following equation:

$$R_{CCM} = {Q_{slow}}/{Q_{tot}} \quad (3)$$

The main disadvantage of the CCM is that the detector's discrimination performance is highly dependent on the choice of the integration periods. However, it is known [18] that each part of the acquisition chain and each parameter setting influences the integral duration values corresponding to optimal discrimination. The usual experimental setup in the laboratory where the CCM is used involves plastic scintillators (with most of the time about the same decay times) and the PMT presented in Section II.A. Therefore, the integration periods have only been optimized for this acquisition chain and are worth 800 ns for the total period and 56 ns for the fast period.

In many applications, multi-radiation fields and numerous measurement systems are encountered, so optimization

methods presented in Section I were not entirely satisfactory for several reasons:

- the need for prior calibration during which the nature of the phenomena at the origin of the detection signal is known by another discrimination method;
- limitations to two types of particles;
- lack of solutions to exclude results that are inconsistent with the physical phenomena involved.

As an example of inconsistent results to be excluded, we can cite the case where, although only one type of particles is involved, an approximation by a function of two Gaussians may be obtained (Fig. 9). With such limitations, an optimization of the integration gates when the detector is exposed to an unknown flux of two or more types of particles is difficult to achieve.

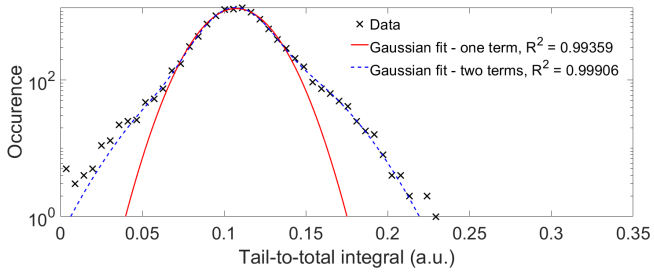

Fig. 9. Example of a fit with a function of two Gaussians when only one particle is involved.

B. *Figure of Merit*

When there are only two origins of pulses, the classical neutron-γ Figure of Merit (FoM), determined from an analysis on the distribution of tail-to-total integrals, is used to assess discrimination capabilities of a scintillator in a defined energy domain [19]. An example, obtained with a mixed neutron-gamma emitting ^{252}Cf source measured through the plastic scintillator and the PMT, of this analysis is shown in Fig. 10. This distribution was fit with a two-component Gaussian function (solid line in Fig. 10). The FoM is then evaluated from the two means (μ_{gamma} and $\mu_{neutron}$) and the two full widths at half maximum ($FWHM_{gamma}$ and $FWHM_{neutron}$) identified by the fit, according to following equation:

$$FoM = \frac{|\mu_{gamma} - \mu_{neutron}|}{FWHM_{gamma} + FWHM_{neutron}} \quad (4)$$

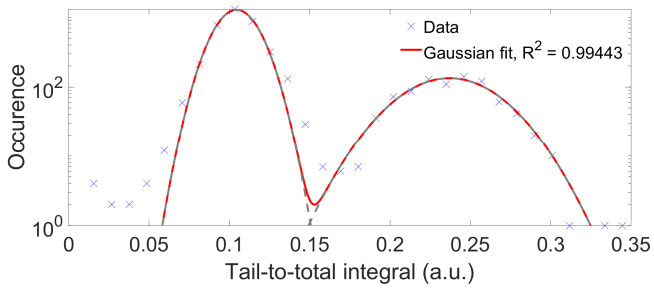

Fig. 10. Example of analysis of a histogram of tail-to-total integrals obtained from a plastic scintillator, a PMT and a ^{252}Cf source.

For applications where more than two components are expected, we propose to use a figure of merit that could include all combinations comparing the discriminating powers between the different particles defined by the following equation:

$$FoM = \sum_{k=1}^{m} \sum_{l=1}^{m} \alpha_{k,l} \frac{|\mu_k - \mu_l|}{w_k + w_l} \quad (5)$$

With:

- $\alpha_{k,l}$, predetermined weighting coefficient associated with a cross contribution of the k-th and the l-th components of the Gaussian function;
- μ_k, μ_l, respectively the mean of the k-th and the l-th components of the Gaussian function;
- w_k, w_l, respectively the FWHM of the k-th and the l-th components of the Gaussian function.

Where the coefficients $\alpha_{k,l}$ are defined according to the measurement objective. An example is given in the Section V.B.

C. *Rejection Ratio*

The relationship between FoM and the probability of pulse classification error, also called rejection ratio (RR), has been identified by Winyard [19]. In the classical neutron/gamma discrimination case, MacDonald [20] described it by (6) and used the intersection of the two Gaussian components as a selection criterion. This rejection ratio uses the complementary error function, denoted $erfc$. Therefore, this implies that the rejection rate evaluated for all measurement systems in this work is based on an idealized Gaussian. As McDonald notes, for high values of the FoM, a rejection ratio computed using (6) will be affected by any non-Gaussian long tails or other artifacts in the peaks. It corresponds to the probability of classifying a gamma interaction as a neutron when its tail-to-total integral is greater than the intersection value. The advantage of using the intersection as a criterion is that the rejection ratio is also equivalent to the probability of classifying a neutron event as a gamma when its tail-to-total integral is lower than the intersection value. This second parameter complements the FoM because it allows a more concrete representation of particles discrimination performance.

$$RR = \frac{1}{2} \cdot erfc(2 \cdot \sqrt{\ln 2} \cdot FoM) \quad (6)$$

For applications where more than two components are expected, the rejection ratio between each kind of particle can be calculated from the distributions evaluated by the Gaussian fit:

$$RR_{k,l} = \int_0^{R_{ip}} D_k(r)dr = \int_{R_{ip}}^1 D_l(r)dr \quad (7)$$

With:

- R_{ip}, intersection point of D_k and D_l;
- D_k, D_l, respectively the distribution of the k-th and the l-th components of the Gaussian function.

D. *Energy calibration*

The pulse distribution as a function of the total integral is exploited for energy calibration of the acquisition chains (here ^{137}Cs and ^{22}Na examples in Fig. 11). It was done for the

following cases: liquid scintillator with PMT, plastic scintillator with PMT and plastic scintillator with SiPM. The results, presented in Section V, for these three measurement systems were performed for energy above 250 keVee. It is not usual to perform an energy calibration for the other two systems: *phoswich* with PMT and fission chambers. The calibration was carried out according to the procedure proposed in [21], [22]. When there were identifiable, we use the Compton edge energies of ^{137}Cs (477 keV) and ^{22}Na (341 keV and 1062 keV) and the photopeaks of ^{241}Am (60 keV), ^{133}Ba (81 keV) and ^{57}Co (122 keV). A linear energy response function was then applied for the calibration.

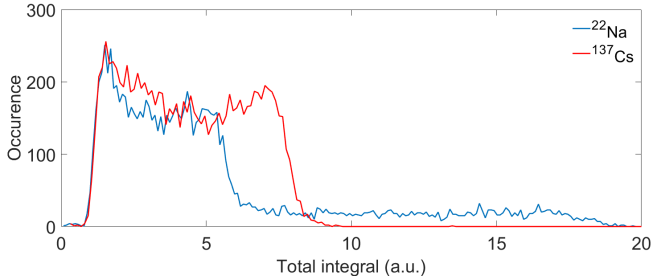

Fig. 11. Examples of spectrum obtained from ^{137}Cs and ^{22}Na sources with a plastic scintillator and a PMT.

Thanks to this energy calibration, the calculation of the FoM value can be performed in a given energy domain in order to assess the impact of the energy on discrimination performance. The bi-parametric histogram presented in Fig. 12 corresponds to the two-dimensional graphical representation of the distribution of tail-to-total integral as a function of the total integral. To highlight densely populated areas, the maximum value of the color level was chosen for a number of five occurrences. Two areas are visible, the top area corresponds to neutron interactions and the bottom area contains the contribution of gamma rays. One can also notice that there are pulses down to about 1 a.u., then none between 0.5 and 1 a.u. and then some between 0.25 and 0.5 a.u. This singular distribution is due to the presence of thermionic emissions of PMT.

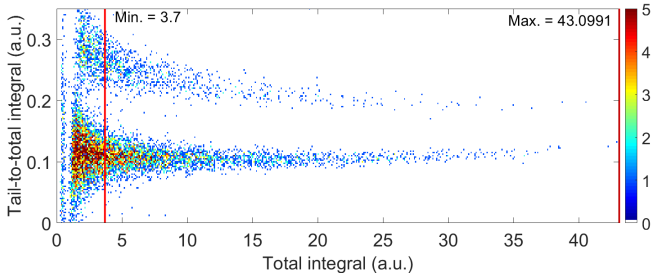

Fig. 12. Example of a bi-parametric histogram of tail-to-total integral as a function of the total integral obtained from a plastic organic scintillator, a PMT and a ^{252}Cf source. The red bars correspond to the limits of the energy range [250 keVee; 4.5 MeVee].

IV. Our Procedure for Optimizing CCM

The goal behind our algorithm development is to identify optimal integration periods by analyzing unclassified detection signals produced by two or more types of particles in order to allow the best use of an acquisition chain without characterizing each part of it. In addition, to solve the problems described in Section III.A, we developed an unsupervised method that:

1. reduces the pre-processed (baseline-subtracted) digitized pulses to two features using two adjustable reduction parameters,
2. combines the two features into one score using CCM,
3. builds a distribution of the score,
4. obtains FoM values by fitting the distribution of scores with Gaussians,
5. optimizes the adjustable reduction parameters with respect to FoM,
6. and reports performance based on RR.

A. *Principle*

The principle of the proposed procedure is divided into three interlocked parts:

- The main program corresponds to the first sequence (top in Fig. 13) and evaluates the FoM for all possible integration periods. From this evaluation, the maximum value of the FoM is identified, the optimal integration periods that led to this value are extracted and the RR is calculated.
- The second sequence (center of Fig. 13) corresponds to the subprogram evaluating the FoM called by the first sequence for each combination of integration periods. Then a set of Gaussian fits whose number of components varies from one to the expected number of components is made on the distribution of the tail-to-total integral. The compliance with an acceptance criterion, the value of which is defined by the user, on the correlation coefficients of all fits is checked and, where applicable, the FoM and rejection ratio calculated.
- The third sequence (bottom in Fig. 13) corresponds to the subprogram of the second sequence verifying compliance with the acceptance criterion in terms of the correlation coefficients of all fits and calculating the FoM. The FoM is only calculated when the correlation coefficient of the Gaussian fit whose number of components is equal to the expected number of components meets the acceptance criterion, otherwise its value is zero.

Fig. 13 represents the procedure in the form of a flowchart, the notations are explained below:

- $t_{fast} = [min; step; max]$, the t_{fast} domain to be tested;
- $t_{slow} = [min; step; max]$, the t_{slow} domain to be tested;
- R_{CCM}, tail-to-total integral;
- N_e, expected number of components;
- FAC, the fit acceptance criterion;
- $R^2[x]$, correlation coefficient of the Gaussian fit with $[x]$ component(s).

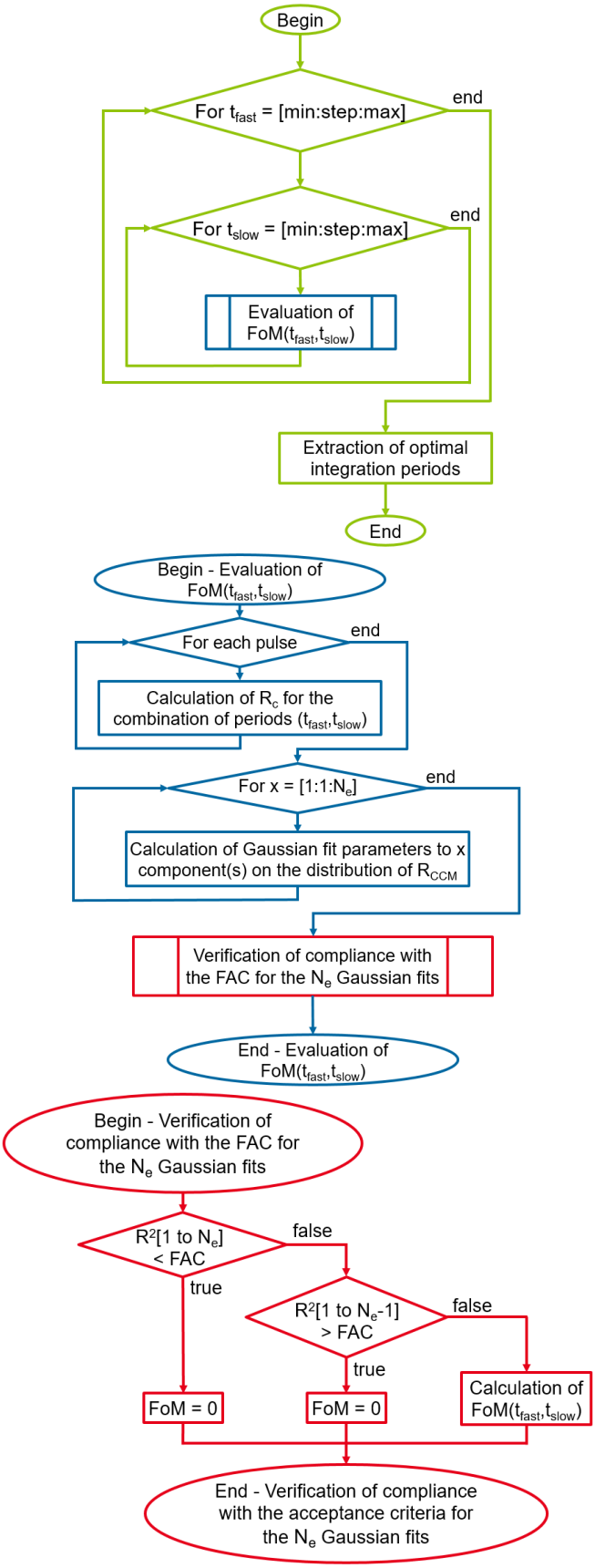

Fig. 13. Procedure for optimizing the CCM.

B. Discussion

In the application cases where the expected number of components is two (such as the classical neutron/gamma discrimination), the FoM and the rejection ratio are calculated according to (4) and (6). When the expected number of components is greater than two, one or more new FoMs are to be defined specifically according to the needs of the experiment. In this case, it is possible to use the FoM and the rejection ratio with (5) and (7) proposed in Section III.

By jointly implementing the conditions on the expected number of components and the correlation coefficient, the procedure is able to discard results that would correspond to a satisfactory approximation with regard to the correlation coefficient, but which would not reflect the physical reality of the involved phenomena.

V. Experimental Result and Discussion

Firstly, we summarized in Table 1, a comparison of the results between the integral periods usually used in the laboratory (56 ns - 800 ns) and the optimal ones found with our procedure.

TABLE 1: Comparison of the results between the integral periods usually used in the laboratory and the optimal ones found with our procedure

Measurement system	Discrimination	Number of components	Usual integral periods				Optimal integral periods			
			t_{fast} (ns)	t_{slow} (ns)	FoM	Rejection ratio	t_{fast} (ns)	t_{slow} (ns)	FoM	Rejection ratio
Plastic scintillator + PMT	Neutron/gamma	2	56	800	1.39	0.05%	75	1050	1.40	0.05%
Liquid scintillator + PMT					0.68	5.47%	22.5	275	1.50	0.02%
Plastic scintillator + SiPM					0.58	8.60%	165	1400	0.88	1.92%
Phoswich + PMT	Beta/gamma	3			0.33	22.02%	11	25	0.85	2.28%
Fission chamber	Neutron/partial discharge	2			1,14	0.36%	170	500	1.85	< 0.01%

Then, the results of our optimization procedure applied to three measurement systems are detailed:

- Neutron/gamma discrimination with the plastic scintillator and the SiPM;
- Discrimination between beta and gamma rays with the *phoswich* organic scintillator and the PMT;
- Discrimination between signal collected from neutron or partial discharge within a fission chamber.

A. Neutron/gamma discrimination with plastic scintillator and SiPM

The result of the optimization of the acquisition chain composed of the plastic scintillator coupled to the SiPM and exposed to a mixed neutron/gamma ^{252}Cf source is shown in Fig. 14. Fig. 15 shows the two-dimensional graphical representation of the distribution of tail-to-total integral as a function of the total integral. The distribution of the tail-to-total integrals for energy deposits greater than 250 keVee (red bar on the left in Fig. 15) and the Gaussian fit obtained for the optimal integration periods are shown in Fig. 16 (left).

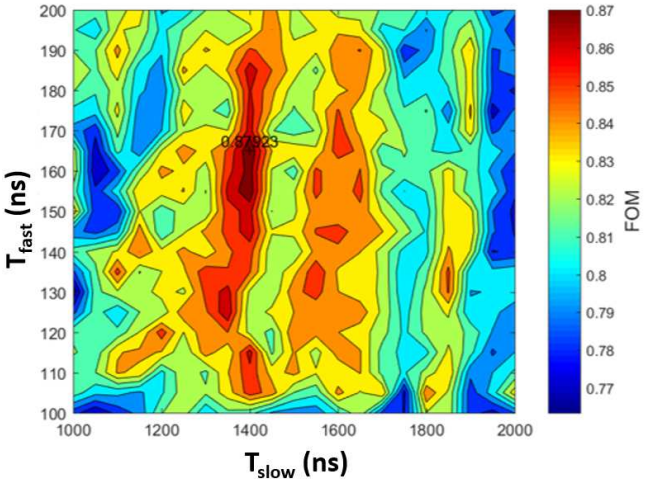

Fig. 14. Example of optimization for neutron/gamma discrimination: FoM value as a function of integration periods obtained from a plastic scintillator, a SiPM and a ^{252}Cf source.

As shown in Fig. 14, the maximum FoM value of 0.88 is obtained for a total integration gate of 1400 ns and a fast integration gate of 165 ns. With such an optimization, the pulses detected with energy above 250 keVee have a rejection ratio of 1.92%. To illustrate the contribution of this optimization procedure to neutron/gamma discrimination performance, on the right in Fig. 16 is the result obtained by using the integration periods usually used in the laboratory. The FoM obtained is 0.58, 34% lower than the optimized one. The rejection ratio would then have been 8.6%.

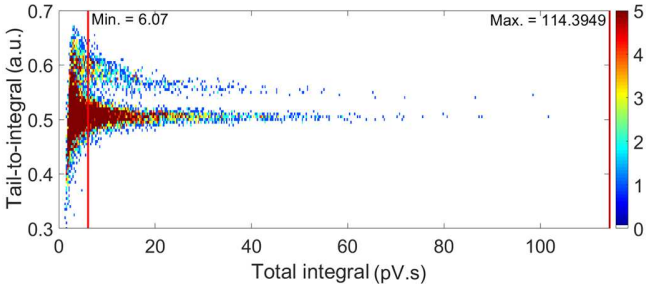

Fig. 15. Bi-parametric histogram of tail-to-total integrals as a function of the total integral obtained from a plastic scintillator, a SiPM matrix and a ^{252}Cf source with the optimized integral durations.

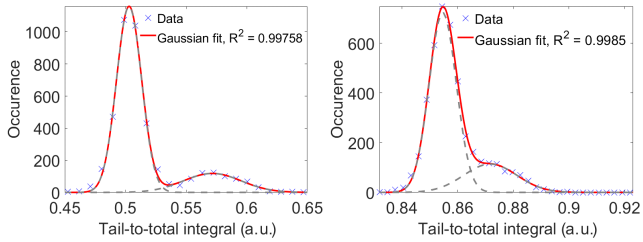

Fig. 16. Histogram of the tail-to-total integrals obtained from a plastic scintillator, a SiPM matrix and a ^{252}Cf source. Left: with optimized integral durations. Right: with the ones usually used in the laboratory.

B. Beta/gamma rays discrimination with phoswich organic scintillator

The application of the CCM optimization procedure applied for the discrimination of beta and gamma rays with a *phoswich* organic scintillator and a PMT exposed to a mixed beta/gamma rays field of ^{137}Cs (only the 662 keV γ-ray was accessible) and ^{90}Sr/^{90}Y sources is shown below in Fig. 17. In our case, it was difficult to differentiate between high-energy beta and gamma rays because of the similar shape of the pulses. Therefore, the coefficients $\alpha_{k,l}$ in (7) were chosen so that the FoM is maximum when the difference between the approximation function corresponding to high-energy betas and the one corresponding to gamma rays is maximum. This means that the coefficient $\alpha_{k,l}$ between high-energy beta and gamma rays is taken equal to 1 and all the other coefficients equal zero.

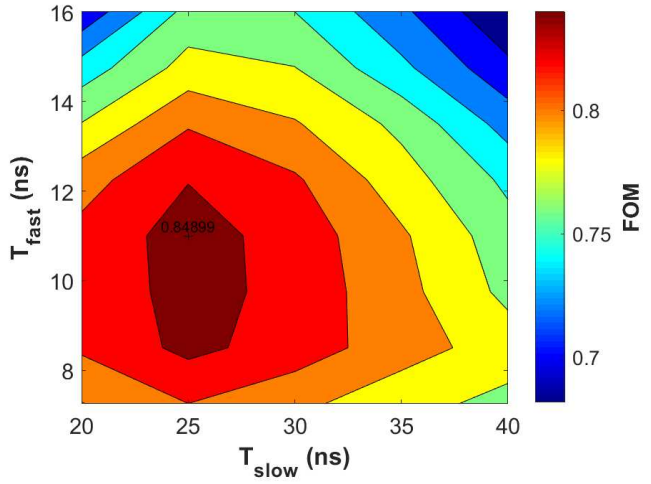

Fig. 17. Example of optimization for high-energy beta and gamma rays discrimination: FoM value as a function of integration periods obtained from a *phoswich* organic scintillator, a PMT, ^{137}Cs and ^{90}Sr/^{90}Y sources.

As shown in Fig. 17, the maximum FoM value of 0.85 is obtained for a total integration gate of 25 ns and a fast integration gate of 11 ns. Fig. 18 shows the two-dimensional graphical representation of the distribution of tail-to-total integral as a function of the total integral. The distribution of the number of pulses as a function of the tail-to-total integral for this combination of optimal integration gates and the Gaussian fit are shown in Fig. 19. With such an optimization, pulses for which the tail-to-total integral is less than about 0.55 have a 98.86% probability of having a beta as their origin. In addition, pulses for which the tail-to-total integral is greater than about 0.55 have a 99.73% probability of having a gamma as their origin.

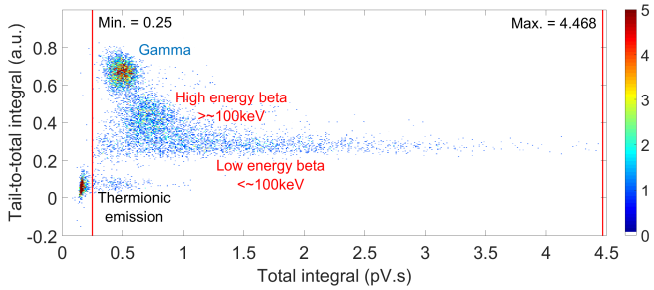

Fig. 18. Bi-parametric histogram of tail-to-total integrals as a function of the total integral obtained from a *phoswich* organic scintillator, a PMT, ^{137}Cs and ^{90}Sr/^{90}Y sources with integral durations optimized for high-energy beta and gamma rays discrimination.

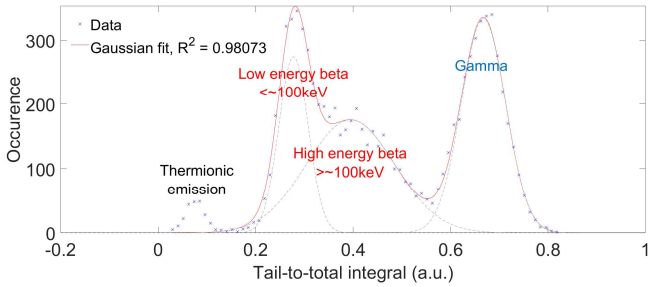

Fig. 19. Histogram of the tail-to-total integral obtained from a *phoswich* organic scintillator, a PMT, a ^{137}Cs and a ^{90}Sr/^{90}Y sources with integral durations optimized for high-energy beta and gamma rays discrimination.

C. Neutron-partial discharge discrimination with fission chamber

This CCM optimization procedure was also applied to High Temperature Fission Chambers. In the experiments performed [17], these chambers were first polarized at 400 V and subjected to a ^{252}Cf neutron source at room temperature, in order to collect the pulses from the neutrons without the interference of the partial discharges. Then, the neutron source was removed and the fission chambers were heated to temperatures between 400 °C and 650 °C, so that the partial discharge pulses could be collected at different temperatures without neutron interference. In this article, to apply the optimization procedure, the two samples were mixed. The result in Fig. 20 shows all the FoMs calculated according to the integration periods, as well as the identification of the optimal periods.

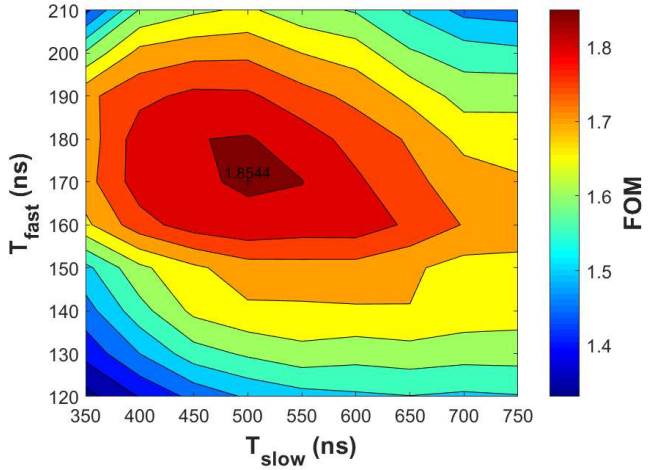

Fig. 20. Example of optimization for neutron-partial discharge discrimination: FoM value as a function of integration periods obtained from a fission chamber at high temperature (650 °C) and a ^{252}Cf source.

As shown in Fig. 20, the maximum FoM value of 1.45 is obtained for a total integration gate of 150 ns and a fast integration gate of 85 ns. Fig. 21 shows the two-dimensional graphical representation of the distribution of tail-to-total integral as a function of the total integral. The distribution of the number of pulses as a function of the tail-to-total integral for this combination of optimal integration gates and the Gaussian fit are shown in Fig. 22. With such an optimization, pulses detected have a rejection ratio of less than 0.01%. To illustrate the contribution of this optimization procedure and the CCM to neutron-partial discharge discrimination, the FWHM was previously [17] used as the feature to discriminate pulses and the rejection ratio was around 1%. The comparison is only made between rejection errors because it is not a usual practice to evaluate the FoM for this kind of acquisition chain.

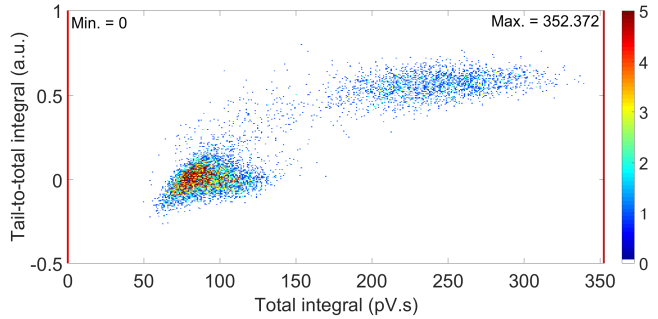

Fig. 21. Bi-parametric histogram of tail-to-total integrals as a function of the total integral obtained from a fission chamber at high temperature (650 °C) and ^{252}Cf source with optimized integral durations.

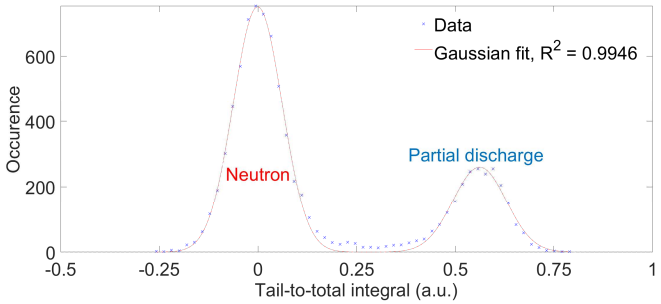

Fig. 22. Histogram of the tail-to-total integral obtained from a fission chamber at high temperature (650 °C) and ^{252}Cf source with optimized integral durations.

VI. Conclusion and Future Work

This paper presents a very simple procedure for optimizing the CCM. Thanks to this procedure, the optimal values of the integration gates are determined automatically and without requiring a prior classification of each pulse of the detection signal. This procedure is independent of the acquisition chain and can be used without full knowledge of how it works.

Thanks to the use of this procedure, we report improvement in FoM for various measurement systems. Besides, a deeper understanding can be investigated by studying the quantity of FoM as provided in Equation (4) from which the improvement is due. Another advantage of the procedure is that it can be adapted to experimental cases where signals of multiple and very different origins can be encountered. This advantage will be particularly interesting in the development of a detector based on a scintillator capable of also discriminating thermal neutrons, fast neutrons and gamma rays. Future work will also include implementing the proposed algorithm on an FPGA to perform real-time optimization and process data at a high acquisition rate.

References

[1] G. F. Knoll, *Radiation Detection and Measurement*, vol. Third edit. 1999.

[2] G. H. V Bertrand, M. Hamel, S. Normand, and F. Sguerra, "Pulse shape discrimination between (fast or thermal) neutrons and gamma rays with plastic scintillators : State of the art," *Nucl. Instruments Methods Phys. Res. A*, vol. 776, pp. 114–128, 2015.

[3] M. Flaska and S. A. Pozzi, "Identification of shielded neutron sources with the liquid scintillator BC-501A using a digital pulse shape discrimination method," vol. 577, pp. 654–663, 2007.

[4] N. Zaitseva *et al.*, "Plastic scintillators with efficient neutron / gamma pulse shape discrimination," *Nucl. Instruments Methods Phys. Res. A*, vol. 668, pp. 88–93, 2012.

[5] S. A. Pozzi, M. M. Bourne, and S. D. Clarke, "Pulse shape discrimination in the plastic scintillator EJ-299-33," *Nucl. Instruments Methods Phys. Res. A*, vol. 723, pp. 19–23, 2013.

[6] P. Blanc, M. Hamel, C. Dehé-Pittance, L. Rocha, R. B. Pansu, and S. Normand, "Neutron/gamma pulse shape discrimination in plastic scintillators: Preparation and characterization of various compositions," *Nucl. Instruments Methods Phys. Res. A*, vol. 750, pp. 1–11, 2014.

[7] N. Zaitseva *et al.*, "Scintillation properties of solution-grown trans - stilbene single crystals," *Nucl. Instruments Methods Phys. Res. A*, vol. 789, pp. 8–15, 2015.

[8] M. Flaska and S. A. Pozzi, "Optimization of an offline pulse-shape discrimination technique for the liquid scintillator BC-501A," *ORNL/TM-2006/120, Oak Ridge National Laboratories*. p. 27, 2006.

[9] Z. Wang, J. Zeng, T. Zhu, Y. Wang, C. Yang, and R. Zhou, "Optimization of integration limit in the charge comparison method based on signal shape function," *Nucl. Instruments Methods Phys. Res. A*, vol. 760, pp. 5–9, 2014.

[10] A. Sardet, "Spectres en énergie des neutrons prompts de fission : optimisation du dispositif expérimental et application à l'^{238}U," Université de Paris-Saclay, 2015.

[11] J. B. Birks, "Scintillations from Organic Crystals: Specific Fluorescence and Relative Response to Different Radiations," *Proc. Phys. Soc. Sect. A*, vol. 64, pp. 874–877, 1951.

[12] R. Voltz and G. Laustriat, "Radioluminescence des milieux organiques - I. Etude cinétique," *J. Phys. Fr.*, vol. 29, pp. 159–166, 1968.

[13] D. H. Wilkinson, "The phoswich - a multiple phosphor," *Rev. Sci. Instrum.*, vol. 23, no. 8, pp. 414–417, 1952.

[14] N. J. Cherepy *et al.*, "Bismuth- and lithium-loaded plastic scintillators for gamma and neutron detection," *Nucl. Instruments Methods Phys. Res. A*, vol. 778, pp. 126–132, 2015.

[15] T. Huang, Q. Fu, C. Yuan, and S. Lin, "A gamma and neutron phoswich read out with SiPM for SPRD," *Nucl. Instruments Methods Phys. Res. Sect. A Accel. Spectrometers, Detect. Assoc. Equip.*, vol. 881, pp. 48–52, 2018.

[16] C. Blanc, "EFR98 - Synthesis on core instrumentation," *EFR C2-06-5-2394(EF16452)*, 1998.

[17] H. Hamrita, C. Jammes, G. Galli, and F. Lainé, "Rejection of partial-discharge-induced pulses in fission chambers designed for sodium-cooled fast reactors," *Nucl. Instruments Methods Phys. Res. A*, vol. 848, no. November 2016, pp. 109–113, 2017.

[18] S. Rawat *et al.*, "Pulse shape discrimination properties of $Gd_3Ga_3Al_2O_{12}$:Ce,B single crystal in comparison with CsI:Tl," *Nucl. Instruments Methods Phys. Res. A*, vol. 840, no. September, pp. 186–191, 2016.

[19] R. A. Winyard, J. E. Lutkin, and G. W. McBeth, "Pulse shape discrimination in inorganic and organic scintillators. I," *Nucl. Instruments Methods*, vol. 95, no. 1, pp. 141–153, 1971.

[20] B. S. Mcdonald *et al.*, "A wearable sensor based on CLYC scintillators," *Nucl. Instruments Methods Phys. Res. A*, vol. 821, pp. 73–80, 2016.

[21] L. Swiderski *et al.*, "Measurement of Compton edge position in low-Z scintillators," *Radiat. Meas.*, vol. 45, pp. 605–607, 2010.

[22] X. Li, Y. Wang, R. Zhou, and C. Yan, "Energy calibration for plastic scintillation detectors based on Compton scatterings of gamma rays," *J. Instrum.*, vol. 12, p. 12025, 2017.